Effect of frustrated exchange interactions and spin-half-impurity on the electronic structure of strongly correlated $NiFe_2O_4$

Kodam Ugendar,[1] S. Samanta,[2] Sudhindra Rayaprol,[3] V. Siruguri,[3] G. Markandeyulu,[1] and B. R. K. Nanda[2,*]

[1]*Advanced Magnetic Materials Laboratory, Department of Physics, Indian Institute of Technology Madras, Chennai 600 036, India*

[2]*Condensed Matter Theory and Computational Lab, Department of Physics, Indian Institute of Technology Madras, Chennai 600 036, India*

[3]*UGC-DAE Consortium for Scientific Research, Mumbai center, Bhabha Atomic Research Centre, Trombay, Mumbai 400 085, India*

(Received 7 March 2017; revised manuscript received 26 June 2017; published 19 July 2017)

Spin-polarized density functional calculations, magnetization, and neutron diffraction (ND) measurements are carried out to investigate the magnetic exchange interactions and strong correlation effects in Yb substituted inverse spinel nickel ferrite. In the pristine form, the compound is found to be a mixed insulator under the Zaanen-Sawatzky-Allen classification scheme as it features both charge transfer and Mott insulator mechanisms. Estimation of magnetic exchange couplings reveals that both octahedral-octahedral and octahedral-tetrahedral spin-spin interactions are antiferromagnetic. This is typical of a spin-frustrated triangular lattice with one of the vertices occupied by tetrahedral spins and the remaining two occupied by octahedral spins. However, since the octahedral-tetrahedral interaction is dominant, it leads to a forced parallel alignment of the spins at the octahedral site which is in agreement with the results of ND measurements. The substituent Yb is found to be settled in +3 charge state, as confirmed from the x-ray photoelectron spectroscopy measurements, to behave like a spin-half-impurity carried by the localized $f_{z(x^2-y^2)}$ orbital. The impurity f spin significantly weakens the antiferromagnetic coupling with the spins at the tetrahedral site, which explains the experimental observation of a decrease in Curie temperature with Yb substitution.

DOI: 10.1103/PhysRevB.96.035138

I. INTRODUCTION

The cubic inverse spinel $NiFe_2O_4$ (NFO) has been extensively investigated in the context of nanomagnetism [1], spin filtering [2,3], spintronics [4], and multiferroics [5]. In addition, it exhibits unusual electronic and magnetic properties when Fe^{3+}/Ni^{2+} ions at the octahedral sites are partially substituted by other transition metal (M) ions, rare-earth (R) ions, or ions of nontransition elements [6–11]. The collinear Néel-type ferrimagnetic structure of NFO yields to a triangular Yafet-Kittel structure upon substantial Cr substitution at the Fe cations at the octahedral sites [6]. The octahedra containing Fe^{3+} ions in NFO, when partially substituted by rare-earth (R^{3+}), become noncentrosymmetric to make the compound ferroelectric. Experimentally it has been shown that substituents such as Sm^{3+} and Ho^{3+} induce magnetoelectric effect in NFO [8].

Significant changes in the electronic, magnetic, and structural behavior of Ni-Zn ferrite upon diluting with several rare-earth ions have been observed [9–11]. With substitution of 2% of Fe by R (=Yb, Er, Dy, Tb, Gd, Sm, and Ce) in $Ni_{0.7}Zn_{0.3}Fe_2O_4$, while lattice has been reported to expand and resistivity has increased, both magnetization and Curie temperature (T_C) have decreased [9–11]. Larger ionic radii of R^{3+} ions cause lattice expansion and the $4f$ electrons are more localized than the itinerant $3d$ electrons and hence, the resistivity increases [9–11]. The reported value of T_C of NFO is 853 K [7,12]. A decrease in T_C upon the partial substitution of R^{3+} for Fe^{3+} in NFO has been reported from our laboratory [7,8]. In $Ni_2Fe_{1.925}R_{0.075}O_4$ compounds, the T_C decreases to 775, 812, and 839 K, respectively, for Dy^{3+} [7], Ho^{3+}, and Sm^{3+} substitutions [8]. However, there are no concrete mechanisms and evidence to explain the decrease in magnetization and Curie temperature, even though qualitatively it has been attributed to weaker R-Fe exchange coupling replacing the stronger Fe-Fe exchange coupling [12,13].

In this paper, results from density functional theory (DFT) calculations and experimental studies are presented and analyzed to explain the electronic and magnetic structures of Yb-substituted NFO, viz., $NiFe_{2-x}Yb_xO_4$ ($x = 0,0.05,0.075$). The reasons for choosing Yb were manifold: (a) Structural distortion is expected to be weak or negligible, since the radius of a Yb^{3+} ion (0.86 Å) is smaller compared to those of the other rare-earth ions. (b) Yb ions can stabilize in +2 and +3 charge states. (c) Yb^{3+} is magnetic and has a lower spin moment compared to the other R^{3+} (R = Gd, Tb, Dy, Ho, Er, and Tb) ions [12] and hence, large reduction in magnetization as well as Curie temperature. (d) Yb^{3+} is expected to provide a spin-half f impurity state. Therefore, it serves as a model system to study the host (d spin)-impurity (f spin) magnetic interactions.

Experimentally, x-ray photoelectron spectroscopy (XPS), Raman spectroscopy, and neutron diffraction (ND) measurements are performed and theoretically, spin-polarized band structure is calculated to explain the electronic structure of $NiFe_{2-x}Yb_xO_4$. In addition, various magnetic exchange couplings are estimated from the total energies of several possible magnetic configurations so that the spin-spin interactions in this compound can be better understood. Emphasis is given on the magnetic coupling of Yb and Fe spins and its effect on the net magnetization as well as T_C of this inverse spinel compound.

The compound NFO behaves as a mixed insulator under the Zaanen-Sawatzky-Allen classification scheme with the trait of both Mott and charge transfer insulating phenomena. It is found that the spins of Fe^{3+} and Yb^{3+} ions at the

*nandab@iitm.ac.in

octahedral sites prefer to align antiparallel. However, stronger antiferromagnetic coupling with the spins at the tetrahedral sites forces them to align parallel in order to avoid spin frustration and thereby stabilizing ferrimagnetism in NFO. The +3 charge state, confirmed from XPS measurements and DFT studies, makes Yb a spin-half ion with the $f_{z(x^2-y^2)}$ orbital carrying the unpaired spin. Experimental observation of the decrease of Curie temperature by approximately 14 K, with 7.5% Yb substitution is attributed to the fact that the Yb spin significantly weakens the antiferromagnetic coupling with the neighboring spins at the tetrahedral site and marginal enhancement of the same with the spins at the neighboring octahedral sites.

The rest of the paper is organized as follows. Sections II and III report experimental and theoretical investigations, respectively. Section II A presents the experimental details involving material synthesis [$NiFe_{2-x}Yb_xO_4$ (x = 0,0.05,0.075)] and characterization. Section II B provides the basic crystal structure information of the Yb-substituted NFO based on x-ray diffraction (XRD) and Raman spectroscopy studies. Section II C analyzes the results from XPS and ND studies. Computational details are reported in Sec. III A, and corresponding results are presented in Sec. III B. In Sec. III C, the magnetic exchange interactions are presented to explain the effect of the Yb-f state on host NFO. Finally, the results are summarized in Sec. IV.

II. EXPERIMENTAL STUDIES

A. Synthesis and characterization of the compounds

Polycrystalline samples of $NiFe_{2-x}Yb_xO_4$ (x = 0,0.05,0.075) were prepared starting from NiO (99.96% pure), Fe_2O_3, and Yb_2O_3 (99.99% pure), by solid-state reaction method. The powders of the starting materials were ground in an agate mortar and pestle for 3 h and heat treated in air at 1200 °C for 12 h. The phase formation of each of the samples was confirmed by taking powder XRD patterns employing a PANalytical (Xpert PRO) x-ray diffractometer with Cu K_α radiation. Raman-active vibrational modes in the samples were recorded using a Horiba Jobin Yvon HR800 UV: Raman Division, Raman spectrometer, with an excitation wavelength of 633 nm, in the wave number range 180–750 cm^{-1}. XPS and ND measurements were carried out on the compound with the highest concentration of Yb, $NiFe_{1.925}Yb_{0.075}O_4$. The Fe 2$p$, Ni 2$p$, Yb 4$d$, and O 1$s$ XPS spectra were recorded with a microfocused monochromatic x-ray source (Design: Sigma Probe) having an energy resolution of 0.47 eV at FWHM. Spectroscopic studies were carried out on thin pellets; the binding energies were charge corrected with reference to C 1s energy level at 284.5 eV. Magnetization data were obtained by employing a vibrating sample magnetometer (VSM; Lakeshore Model 7450). ND experiments were carried out at the Dhruva reactor of Bhabha Atomic Research Center, Trombay, employing the powder diffractometer-3 (λ = 1.48 Å).

B. Structural properties

The structural details, listed in Table I, are obtained through Rietveld refinement using the General Structure Analysis System (GSAS) program. As expected, it is found that for all doping concentrations, the compounds were crystallized in the cubic inverse spinel phase ($Fd\bar{3}m$). However, orthorhombic $YbFeO_3$ appears as the secondary phase. The weight fractions (i.e., phase fractions of different phases present in the compound) of the inverse spinel phase and the secondary phase, respectively, are found to be 0.95 and 0.05 for x = 0.05 and 0.91 and 0.09 for x = 0.075.

The conventional unit cell of NFO comprises 8 divalent cations (Ni^{2+}), 16 trivalent cations (Fe^{3+}), and 32 oxygen anions (O^{2-}). There are two cationic sites in spinel structure: (i) tetrahedrally coordinated A site (T_d symmetry with Wyckoff position 8a) and (ii) octahedrally coordinated B site (O_h symmetry with Wyckoff position 16d). In inverse spinel NFO, A sites are occupied Fe^{3+} cations, and B sites are occupied by both Ni^{2+} and Fe^{3+} cations with equal distributions.

For Yb-doped NFO, the Rietveld refinement was carried out by providing Yb occupancy in place of Fe in both the A site and the B site. The χ^2 value for A-site occupancy is found to be greater than 3 for both the doping concentrations, whereas it is less than 2 for B-site occupancy. This suggests that the Yb^{3+} ion prefers to replace the octahedral Fe^{3+} ion. The replacement of Ni^{2+} by Yb is not favored as the XPS

TABLE I. Structural parameters of $NiFe_{2-x}Yb_xO_4$ (x = 0,0.05,0.075). Here A and B represent the tetrahedral and octahedral sites, respectively.

Composition		x = 0	x = 0.05	x = 0.075
χ^2 (goodness of fit) (B site)		1	1.13	1.21
χ^2 (A site)		1	4.73	3.20
ω_{rp} (weighted refined parameter)		1.68%	1.60%	1.99%
Lattice constant (Å) [14]		8.341(5)	8.343(6)	8.346(3)
Weight fractions [14]	Inverse spinel	1	0.95	0.91
	Secondary phase ($YbFeO_3$)	0	0.05	0.09
Bond length (Å)	O^{2-}-Fe^{3+} (B)	2.032	2.043	2.075
	O^{2-}-Fe^{3+} (A)	1.9	1.882	1.827
Bond angle (degrees)	Fe^{3+} (A)-O^{2-}-Fe^{3+}/Yb^{3+} (B)	123.11	123.54	124.82
	Ni^{2+}-O^{2-}-Ni^{2+}	93.00	92.42	90.62
	O^{2-}-Fe^{3+} (A)-O^{2-}	109.47	109.47	109.47
	O^{2-}-Fe^{3+} (B)-O^{2-}	93.08	92.47	90.62

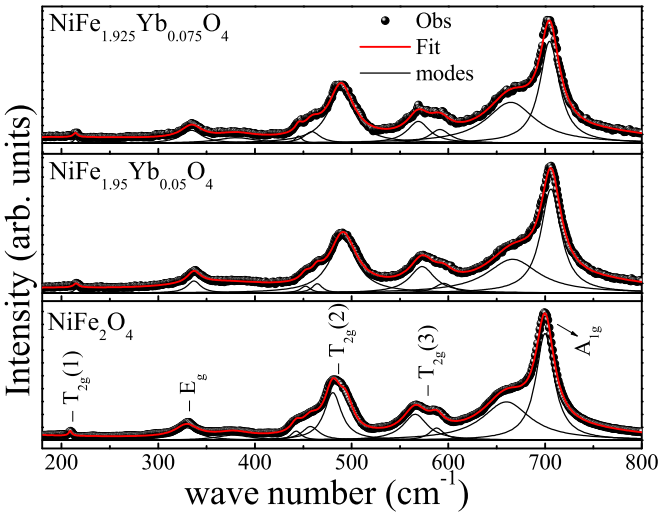

FIG. 1. Raman modes of $NiFe_{2-x}Yb_xO_4$ ($x = 0, 0.05, 0.075$) confirm the single phase inverse spinel structure.

studies, discussed next, suggest a 3+ charge state to Yb. Table I shows that, in agreement with earlier reports [7–10], an increment in the lattice constant was observed for the doped compounds which is attributed to the larger ionic radius of Yb^{3+} (0.86 Å) compared to that of Fe^{3+} (0.63 Å). Also from Table I, it is clear that the octahedral (O-B) bond length has increased and the tetrahedral (O-A) bond length has decreased with Yb substitution. This implies that the Yb^{3+} ions have replaced the Fe^{3+} ions at the octahedral site in the process of doping.

In order to confirm that the compounds formed in inverse spinel structure and that no other phases such as NiO or α-Fe_2O_3 or Fe_3O_4 are present, the materials were further investigated by taking Raman spectra. Figure 1 shows the room temperature Raman spectra recorded in the wave number range 180–750 cm^{-1}. Five Raman modes, viz., A_{1g} (1), E_g (1), T_{2g} (3) corresponding to the inverse spinel phase with space group ($Fd\bar{3}m$) [15,16] were identified and indicated in Fig. 1. Additional peaks, observed in all the compounds, are attributed to the presence of short-range ordering of Ni^{2+} and Fe^{3+} ions at the B site [15–17].

C. Charge state and local spin moments: XPS and ND studies

While majority of the lanthanide elements stabilize in the +3 charge state, Yb stabilizes in both +2 and +3 charge states [18,19]. In order to confirm the charge state of Yb and other cations, XPS measurements were carried out. The Fe 2p and Yb 4d spectra of $NiFe_{1.925}Yb_{0.075}O_4$ are shown in Figs. 2(a) and 2(b), respectively. The Fe 2p spectrum consists of spin-orbit-split $2p_{3/2}$ and $2p_{1/2}$ peaks. The binding energies (BEs) corresponding to both these peaks are in good agreement with literature [20,21]. The peaks also consist of doublets, which were attributed to Fe^{3+} and Fe^{2+} ions.

The high BEs of 712 eV (in the $2p_{3/2}$ peak) and 726.7 eV (in the $2p_{1/2}$ peak) correspond to Fe^{3+} ions. The BEs 709.3 eV (in the $2p_{3/2}$ peak) and 722.5 eV (in the $2p_{1/2}$ peak) correspond to Fe^{2+} ions. This suggests that there exists a minor fraction of Fe^{2+} ions in the synthesized sample. It may be noted that

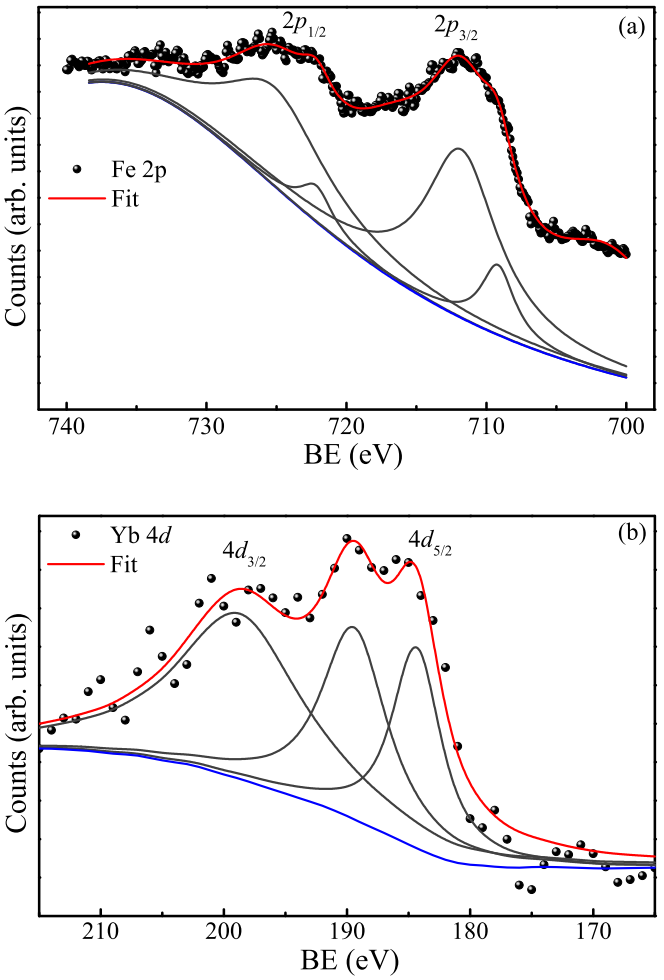

FIG. 2. Fe 2p and Yb 4d core level XPS of $NiFe_{1.925}Yb_{0.075}O_4$.

the Fe BEs corresponding to the +2 and +3 charge states are 709.2 and 711.2 eV, respectively [21]. Droubay and Chambers [20], by analyzing Fe 2p XPS spectra of α-Fe_2O_3 films and Fe 2p (L-edge) x-ray absorption spectra of Fe_2O_3 (in the form of pressed pellet), have reported similar BEs which they attribute to the $2p^5 3d^6 L$ final state of Fe^{3+} ions.

The XPS spectrum of Ni 2p (not shown) exhibits spin-orbit-split $2p_{3/2}$ and $2p_{1/2}$ peaks at 855 and 874 eV, respectively. These binding energies are comparable to that of octahedral Ni^{2+} found in NiO [21–23], suggesting the +2 charge state of Ni, in the compound investigated. The XPS of Yb 4d is shown in Fig. 2(b). The two peaks centered at 184.5 and 199 eV are assigned, respectively, to $4d_{5/2}$ and $4d_{3/2}$ spin-orbit-split 4d levels. These values are in good agreement with that of the Yb 4d level binding energy in Yb_2O_3 [24] which implies a +3 charge state for Yb [24]. The spin-orbit split was found to be 14.5 eV, which further confirms the +3 charge state for Yb. Had it been in a +2 state, the separation would have been 8.8 eV, as suggested by Hagström *et al.* [25]. The O 1s spectrum (not shown) consists of two peaks at 528.8 and 531.9 eV, which are ascribed to O^{2-} ions at the octahedral coordinates and tetrahedral coordinates, respectively.

In order to understand the magnetic ordering and to quantify the local spin moments in $NiFe_{2-x}Yb_xO_4$, ND

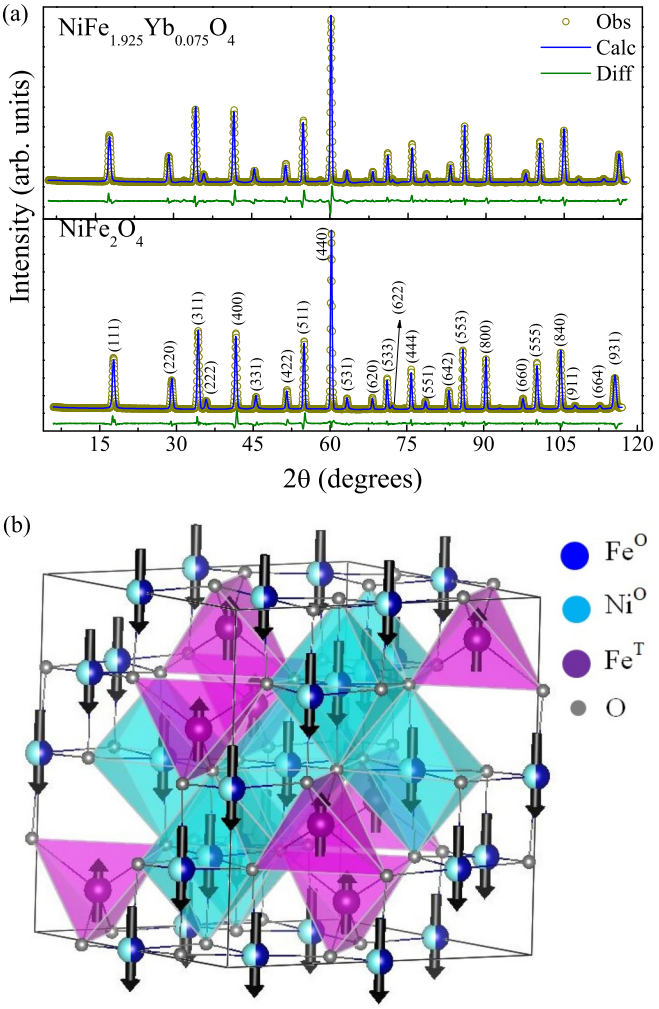

FIG. 3. (a) Indexed Rietveld refined ND pattern of $NiFe_{1.925}Yb_{0.075}O_4$ at 300 K. (b) Magnetic structure confirming the ferrimagnetic nature.

measurements were carried out. The ND patterns recorded at room temperature are shown in Fig. 3(a). Rietveld refinement was done using the FULLPROF program. The site positions used were A site (Fe^{3+}) at $8a$ ($\frac{1}{8},\frac{1}{8},\frac{1}{8}$), B site (Ni^{2+},Fe^{3+},Yb^{3+}) at $16d$ ($\frac{1}{2},\frac{1}{2},\frac{1}{2}$), and oxygen at $32e$ (0.26,0.26,0.26). Thompson-Cox-Hastings pseudo-Voigt function was employed for the peak profile. All the peaks were reconciled with the cubic inverse spinel structure ($Fd\bar{3}m$) and no impurity phase was observed. We would like to note that, as the ND scattering factor is independent of atomic number (Z) the impurity phases with very low phase fraction may not be detected with this technique. However, if the impurity phase has a heavier element as in the case of $YbFeO_3$, it can be detected in XRD measurement where the scattering factor increases with Z. Both the crystal and magnetic refinement parameters are listed in Table II.

From Table II, it can be noted that the magnetization decreases upon substitution of Yb^{3+}. This decrease in magnetization is due to the smaller value of the magnetic moment of Yb^{3+} (0.86 μ_B) compared to that of the Fe^{3+} ion (5 μ_B). This behavior is in agreement with the literature which was obtained

TABLE II. Structural and magnetic parameters of NFO and $NiFe_{1.925}Yb_{0.075}O_4$ as obtained from ND studies.

Compound			NFO	$NiFe_{1.925}Yb_{0.075}O_4$
Lattice constant (Å)			8.3402(3)	8.3446(1)
	χ^2		1.45	1.71
Bragg-R	Bragg-R		5.29	3.85
factors	R_f factor		3.20	3.58
	Mag-R		9.95	8.58
Reliability	R_p		5.37	6.79
factors (%)	R_{wp}		7.87	8.92
	$R_{\exp}$		6.54	6.84
	A site	Fe^{3+}	2.64	2.56
Magnetic	B site	Fe^{3+}	−4.32	−4.15
moments		Ni^{2+}	−1.22	−0.88
(μ_B/f.u.)		Yb^{3+}	-	−0.06[a]
		Net	−5.54	−5.10
Net moment $\lvert\mu_B - \mu_A\rvert$			2.90	2.54

[a]As each f.u. contains 7.5% of Yb, the moment per Yb ion is 0.86 μ_B.

by M-H curves and Mössbauer studies on $NiFe_{2-x}Yb_xO_4$ ($x = 0$, 0.05, and 0.075) [14]. In addition, the substitution of rare-earth ions (possessing a high magnetic moment compared with Fe^{3+}) such as R^{3+} (R = Dy, Gd, Sm, and Ho) in NFO also caused a decrease in magnetization, which has been attributed to antiparallel alignment of R^{3+} (R = Dy, Gd, Sm, and Ho) to octahedral Fe^{3+} moments [7,8,26].

However, in the present case, the moments within the B site, viz., Yb^{3+}, Fe^{3+}, and Ni^{2+} moments, are parallel (Table II). In addition, the moments of Fe^{3+} ions at the A site and that of B site moments (Ni^{2+}, Fe^{3+}, and Yb^{3+}) are antiferromagnetically aligned, and the latter possessing higher moment than the former confirms the ferrimagnetic ordering. The magnetic structure determined from the ND measurements is presented in Fig. 3(b).

The magnetization, measured at a field of 100 Oe, in the temperature range 300–900 K is shown in Fig. 4. The Curie temperature was extracted from the inflection point (in M vs T) which gives a minimum in $\frac{dM}{dT}$ vs T at $T = T_C$ [shown in Fig. 4(b)]. The T_C of $NiFe_{2-x}Yb_xO_4$ compounds were found to be 850, 837, and 836 K, respectively, for $x = 0$, 0.05, and 0.075. For the undoped compound, our result is in close agreement with the reported value of $T_C = 853$ K [7,12]. With Yb substitution in NFO, the T_C drops from 850 to 836 K. In the subsequent section, the strengths of various magnetic exchange interactions in this compound are examined, to understand the reason for the decrease in T_C.

III. ELECTRONIC STRUCTURE FROM DFT STUDIES

To study the formation of Yb impurity spin and its interaction with the host magnetic ordering and thereby to understand the origin behind the experimental observation of a decrease in magnetization and T_C, in this section DFT calculations were carried out and the results are presented in the subsequent sections.

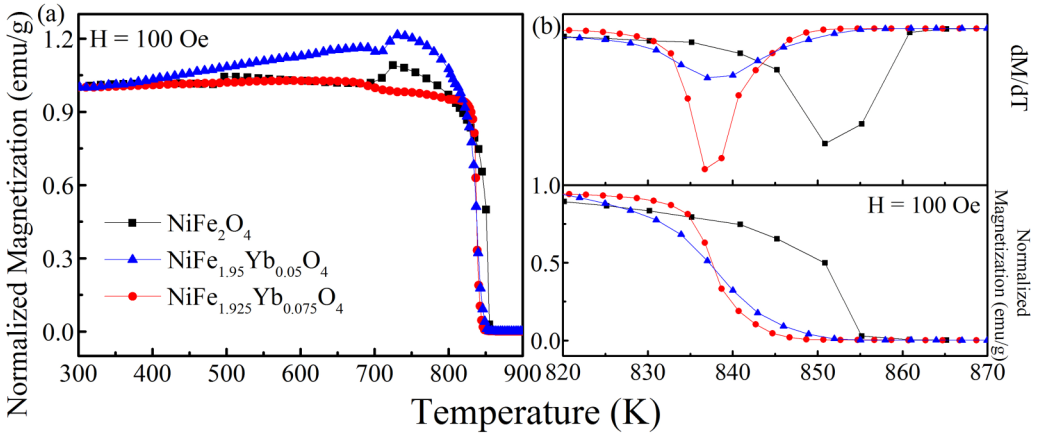

FIG. 4. (a) Magnetization as a function of temperature for $NiFe_{2-x}Yb_xO_4$ ($x = 0, 0.05, 0.075$). (b) Top: $\frac{dM}{dT}$ vs T near T_C. Bottom: M vs T near T_C. The inflection point (in M vs T) implies a minimum in $\frac{dM}{dT}$ vs T at $T = T_C$, which decreases with substitution of Yb.

A. Computational details

The *ab initio* calculations are performed using the full potential linearized augmented plane wave method with local orbital basis (FP-LAPW + lo), as implemented in WIEN2k [27]. For NFO, there are three possible Ni/Fe cation distributions at the B sites, viz., $P\bar{4}m2$, $P4_122$, and $Imma$ [28]. However, it has been found that while the $P\bar{4}m2$ configuration has higher energy, both $P4_122$ and $Imma$ configurations are lower in energy and almost have the same ground state [17]. Since the primitive unit cell of the $P4_122$ configuration consists of four formula units compared to the two formula unit cell for $Imma$, the latter was used for calculations [3]. As mentioned earlier, the octahedral sites are occupied equally by Fe^{3+} and Ni^{2+} ions. Even though the distribution of these ions is random in an experimentally synthesized sample, for computation, ordered distribution with Ni^{2+} and Fe^{3+} ions occupying alternate octahedral sites was considered. The experimental structure was further optimized to study the ground-state electronic and magnetic properties.

For the self-consistent calculations the plane-wave cutoff $RK_{\max}$ was taken to be 7.0 which yielded 3939 plane waves for the interstitial region. The muffin-tin radii of Ni, Fe, Yb, and O were taken as 1.88, 1.84, 1.97, and 1.58 a.u., respectively. For the computation of non-muffin-tin matrix elements, $L_{\max}$ was set to 4. The local orbitals included 4s and 3d states for Ni and Fe; 4f, 6s, and 5d for Yb; and 2s and 2p states for O. Brillouin zone integration was performed using the tetrahedron method on an $8 \times 8 \times 8$ k grid. Out of the possible exchange-correlation approximations, such as local spin-density approximation (LSDA) [29], LSDA+SIC (self-interaction correction) [30], generalized gradient approximation (GGA) [31], and GGA+U [3] applied to NFO so far, the result with GGA+U matched well with the experimental magnetic ordering as well as band gap [32]. Therefore, the results presented in this paper are obtained within the framework of GGA+U. The effective U (i.e., $U - J = 3$ eV) is applied to the Ni-d, Fe-d, and Yb-f orbitals and the calculations are carried out using a rotationally invariant Dudarev approach [33]. Supporting the experimental observation, the calculations showed that Yb replacing the octahedral Fe (Fe^O) is more favorable by 0.6 eV than Yb replacing the tetrahedral Fe (Fe^T). Therefore, in the rest of the paper, the results for $NiFe^O_{1-x}Yb_xFe^TO_4$ are presented.

For the electronic structure calculations with substituents, a $2 \times 2 \times 2$ supercell which gives rise to a 16 f.u. unit cell was constructed. One and two Yb atoms were substituted to construct $NiFe_{2-0.0625}Yb_{0.0625}O_4$ and $NiFe_{2-0.125}Yb_{0.125}O_4$, respectively. Even though these concentrations of Yb ions do not match exactly with those of the synthesized samples, $NiFe_{2-0.05}Yb_{0.05}O_4$ and $NiFe_{2-0.075}Yb_{0.075}O_4$, the qualitative features of Yb substitution are not expected to differ substantially. The optimized lattice constants of $NiFe_{2-x}Yb_xO_4$ are found to be 8.44, 8.46, and 8.53 Å for $x = 0$, 0.0625, and 0.125, respectively. These agree well with experimental observation of lattice expansion with substitution of Yb.

B. Electronic and magnetic structures of pure and Yb-doped NFO

The electronic structure of pure NFO has been investigated by many in the past in the context of strong correlation effects [32,34], spin-filter efficiency [3], and stability of normal and inverse spinel configurations [17,30,31]. In the present study, the electronic structure of NFO is revisited in order to examine the effect of substitution of Yb as well as to explain the insulating mechanism of the parent compound.

In NFO, due to the octahedral crystal-field effect of O ligands, Ni and Fe^O-d states are split into triply degenerate t_{2g} and doubly degenerate e_g states with the former lying lower in energy. Likewise, the tetrahedrally coordinated Fe-d states are split into doubly degenerate e and triply degenerate t_2, where the latter has higher energy. The densities of states (DOS) in Fig. 5 show these crystal-field effects. From the figure, it can also be seen that in the spin-up channel, both t_{2g} and e_g states of Ni and Fe^O are occupied. However, in the spin-down channel, the Fe^O-d states are empty and only Ni-t_{2g} states are occupied. On the other hand, the spin-resolved occupancy of the Fe^T-d states is opposite to that of Fe^O. These occupancies together confirm Ni^{2+} and Fe^{3+} charge states and also the antiparallel alignment of Fe^T spins with Ni and Fe^O spins. Such a spin alignment makes NFO ferrimagnetic with a net

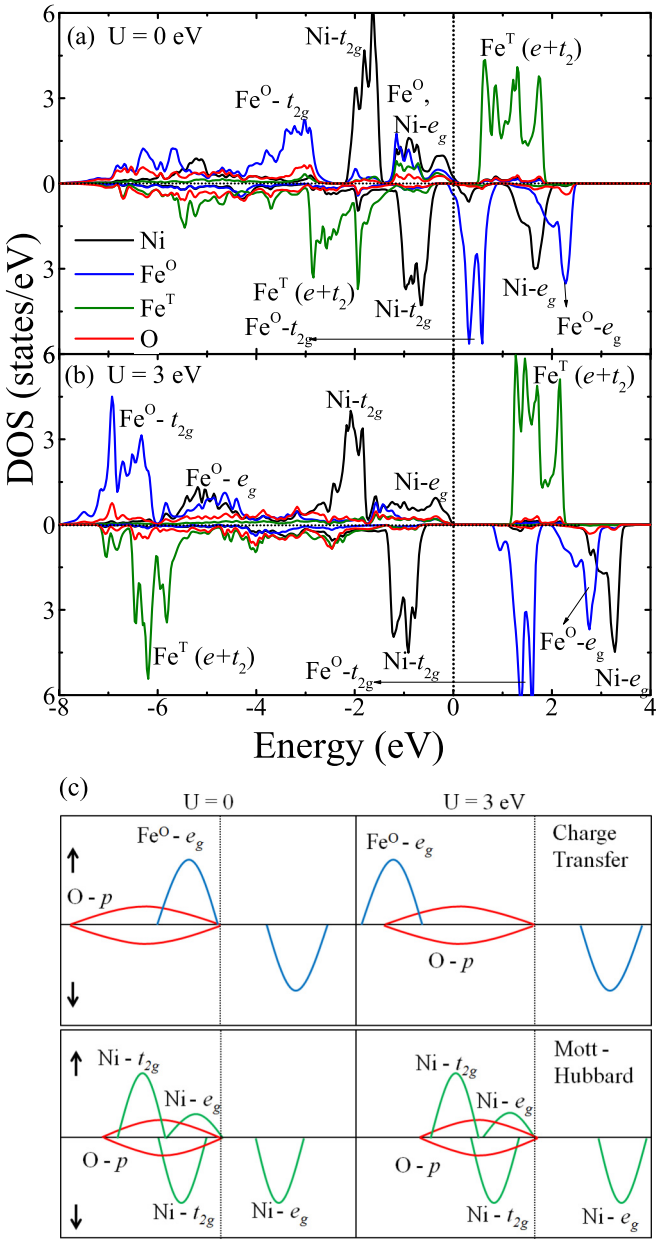

FIG. 5. Spin-polarized DOS of NFO using (a) GGA and (b) GGA+U show that the correlation effect makes the system insulating. (c) Schematic diagram illustrating the insulating mechanism in this compound.

TABLE III. The local magnetic moment (estimated within the muffin-tin sphere) of Ni, Fe^{O}, Yb, and Fe^{T} of $NiFe_{2-x}Yb_xO_4$ ($x = 0$, 0.0625, and 0.125) using GGA+U(= 3 eV).

	Moments (μ_B/f.u.)		
Composition	$x = 0$	$x = 0.0625$	$x = 0.125$
Ni	1.57	1.57	1.58
Fe^{O}	3.98	3.98	4.07
Fe^{T}	−3.83	−3.83	−3.93
Yb		0.90	0.90
O	0.06	0.05	0.04
Total	2.00	1.75	1.50

magnetic moment of 2 μ_B/f.u. (see Table III), which is in agreement with those reported in literature [7,8,12,14,35].

In order to examine the role of strong correlation effect on the insulating behavior, the partial densities of states obtained using GGA and GGA+U are shown in Figs. 5(a) and 5(b), respectively. Since Ni-t_{2g} states are occupied in both the spin channels, they are not affected by the on-site repulsion U. The half-filled Fe^{O}-d states exhibit maximum strong correlation effect. Specifically, the Fe^{O}-e_g spin-up states, which are at the Fermi level (E_F) along with O-p states in GGA, are now pushed down in energy, with the inclusion of U. Since O-p states occupy the E_F, it confirms the charge-transfer mechanism. However, the same is not the case for Ni-e_g states. In the spin majority channel, the band center of Ni-e_g lies above the band center of O-p in order to favor the Mott-Hubbard mechanism. The Fe^{T}-d states are away from the E_F both in GGA and GGA+U and hence, have a negligible role in determining the insulating mechanism in this system. As a whole, the entire system behaves as a mixed insulator falling under the Zaanen-Sawatzky-Allen classification scheme [36]. The insulating mechanism in this compound is summarized schematically in Fig. 5(c). We find that the mechanism remains valid for higher values of U.

With Yb substitution at the octahedral site, it was found that, both within GGA and GGA+U, Yb did not affect the Ni and Fe d states and hence, only the Yb-f partial DOS is plotted in Fig. 6. The GGA-only calculation shows two prominent peaks near E_F which are denoted as (a) and (b). These peaks together form partially occupied f states and from the charge density plot, shown in Fig. 6, they are found to be linear combinations of f_{z^3} and $f_{z(x^2-y^2)}$ states. The rest of the f orbitals lie lower in energy and are completely occupied. This can be understood from crystal-field effect. As Yb^{3+} is in an octahedral site and these f orbitals are nearly along the axis of the YbO_6 octahedra, they experience stronger Coulomb repulsion by the O ligands, compared to the rest and hence, lie higher in energy.

The strong correlation effect splits these partially occupied states to lower Hubbard band (LHB) and upper Hubbard band (UHB) which are also reflected in the DOS obtained with $U = 3$ eV. In Fig. 6(i) the peak (c) constitutes the LHB and the peak (d) constitutes the UHB. From the electronic density plot shown in Fig. 6(ii), LHB is found to be of f_{z^3} character and UHB is found to be of $f_{z(x^2-y^2)}$ character. Since in the spin-majority channel Yb-f states are completely occupied and in the spin-minority channel only $f_{z(x^2-y^2)}$ is empty, this further reveals that Yb is in the +3 charge state, confirming the experimental observation.

C. Magnetic exchange interactions of pure and Yb-substituted compound

While studying the magnetization as a function of temperature in Fig. 4, it was found that the Yb substitutions led to a decrease in the Curie temperature of the ferrimagnetic ordering. Since T_C is determined from the spin-exchange interaction strengths J, it is imperative to identify the dominant interaction paths in the NFO and how they are affected by substitution of Yb. In this section, the Heisenberg Hamiltonian $H = -\sum_{i,j} J_{ij} \vec{S}_i \cdot \vec{S}_j$ was employed to $NiFe_{2-x}Yb_xO_4$ ($x =$

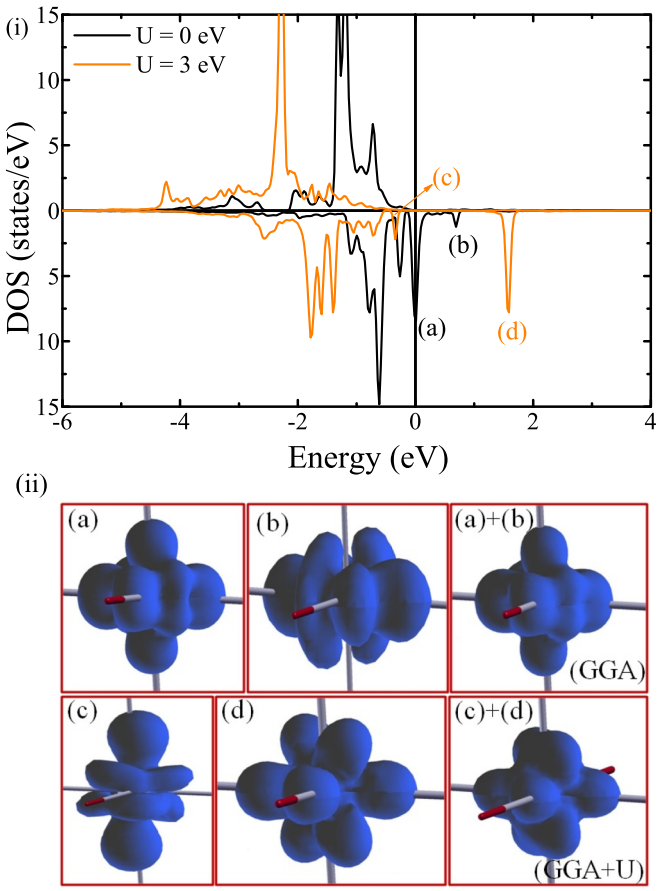

FIG. 6. (i) Partial Yb-f DOS for $NiFe_{2-0.0625}Yb_{0.0625}O_4$. The partially occupied states ($U = 0$) split to form occupied lower Hubbard and unoccupied upper Hubbard bands under the influence of U. (ii) The electronic charge densities of the partially occupied states ($U = 0$) and the lone unoccupied states ($U = 3$ eV) are also shown.

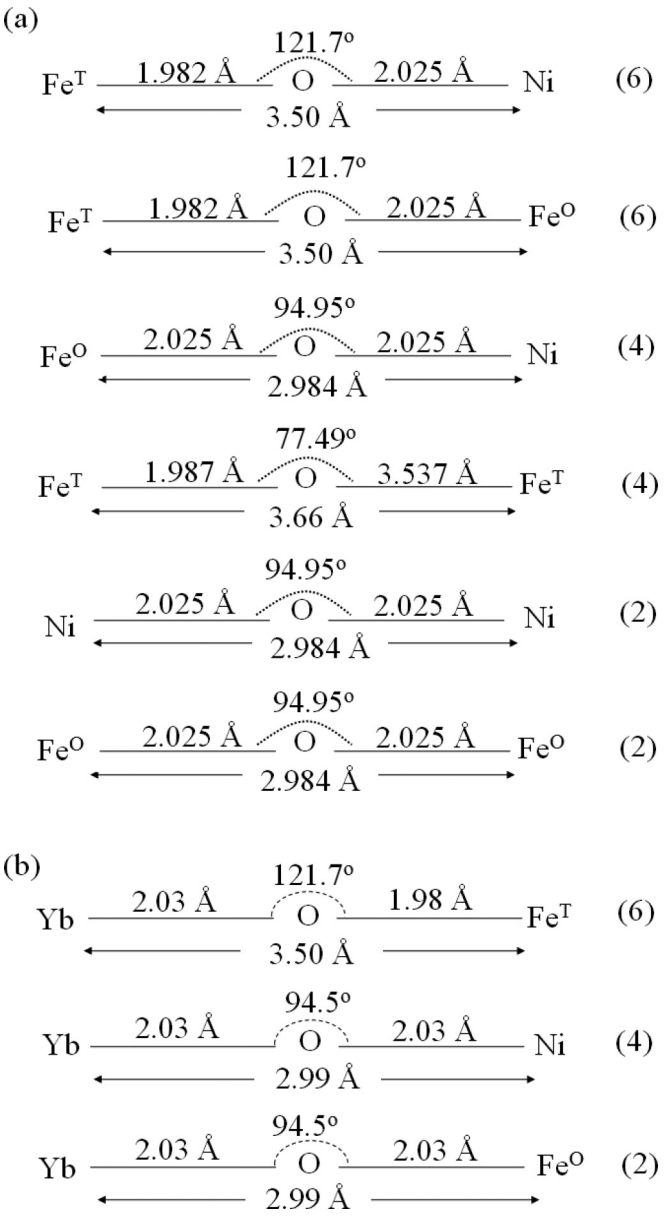

FIG. 7. (a) Several exchange paths between the transition metal cations via the oxygen anion considered for NFO. The maximum cation-cation separation is restricted to 3.66 Å. The larger exchange paths are ignored as the coupling strength of them is expected to be negligible. (b) For $NiFe_{2-0.0625}Yb_{0.0625}O_4$, only three different exchange paths are taken into account. The number written within the parentheses (extreme right) implies the number of such identical exchange paths from the reference spin.

0,0.0625) compounds over several exchange paths between the transition metal cations, as shown in Fig. 7. The value of J_{ij} between two neighboring spins S_i and S_j of the dimer i-j was obtained from the relation $J_{ij} = E_{i\uparrow j\downarrow} - E_{i\uparrow j\uparrow}$. Here, E is the energy of the corresponding spin configurations and was evaluated from DFT calculations. Since multiple intercoupled spin dimers are involved in this system, the energies of several configurations were calculated to get the values of J's.

For NFO, six exchange interaction paths, as shown in Fig. 7(a), were considered and therefore, a minimum of seven magnetic configurations were necessary. Table IV lists these seven configurations as well as the relation between the J_{ij} and E of these configurations. Simultaneous solutions of these relations give the values of J_{ij} which are given in Table V. The results are comparable to those obtained by Srivastava *et al*. [37] and by Cheng [38]. The former has estimated J using the Anderson transfer integral [39] as well as a three-sublattice model. They have found that the strongest exchange interaction is $J_{Fe^OFe^T}$ which is in agreement with our study. In addition, except J_{NiNi}, the signs of the exchange interactions are also found to be the same. Only three J values (J_{NiFe^O}, J_{NiFe^T}, $J_{Fe^TFe^O}$) have been estimated by Cheng [38], by pseudopotential-based DFT calculations and the present results are in good agreement with them [38].

Table V suggests that each of the exchange interactions is antiferromagnetic in nature (as shown in Fig. 8). However, the ground-state magnetic ordering shows that the spins at the octahedral sites (henceforth referred to as octahedral spins) are aligned parallel and there is an antiparallel alignment between the octahedral and tetrahedral spins. This can be explained from the schematic triangles (see Fig. 8) representing the magnetic coupling between two octahedral spins and one

TABLE IV. (Pure) The seven magnetic configurations and the relation between the corresponding total energies and six exchange interactions [see Fig. 7(a)] evaluated in this work. The equations are obtained by keeping the spin at one of the Fe^O sites (termed as reference spin) fixed and flipping the neighboring Ni, Fe^O, and Fe^T spins as indicated in the table. (Yb substituted) In the case of Yb substitution, four necessary configurations are considered so that J_{YbNi}, J_{YbFe^O}, and J_{YbFe^T} [see Fig. 7(b)] can be evaluated.

Configurations	Ref. spin	Flipped spins			
pure (NFO)	Fe^O	Ni	Fe^O	Fe^T	Energy difference
1	↑	↑	↑	↓	E_1 (ground state)
2	↑	↓	↑	↓	$E_2 - E_1 = 4J_{NiNi} + 8J_{NiFe^O} - 12J_{NiFe^T}$
3	↑	↑	↓	↓	$E_3 - E_1 = 8J_{NiFe^O} + 4J_{Fe^OFe^O} - 12J_{Fe^OFe^T}$
4	↑	↑	↑	↑	$E_4 - E_1 = -12J_{NiFe^T} - 12J_{Fe^OFe^T} + 8J_{Fe^TFe^T}$
5	↑	↓	↓	↓	$E_5 - E_1 = 4J_{NiNi} + 12J_{NiFe^O} - 12J_{NiFe^T} + 4J_{Fe^OFe^O} - 12J_{Fe^OFe^T}$
6	↑	↓	↑	↑	$E_6 - E_1 = 4J_{NiNi} + 8J_{NiFe^O} - 20J_{NiFe^T} - 12J_{Fe^OFe^T} + 8J_{Fe^TFe^T}$
7	↑	↑	↓	↑	$E_7 - E_1 = 8J_{NiFe^O} - 12J_{NiFe^T} + 4J_{Fe^OFe^O} - 20J_{Fe^OFe^T} + 8J_{Fe^TFe^T}$
Yb substituted	Yb	Ni	Fe^O	Fe^T	
1	↑	↑	↑	↓	E'_1 (ground state)
2	↑	↓	↑	↓	$E'_2 - E'_1 = 4J_{NiNi} + 6J_{NiFe^O} - 12J_{NiFe^T} + 2J_{YbNi}$
3	↑	↑	↓	↓	$E'_3 - E'_1 = 2J_{Fe^OFe^O} + 8J_{NiFe^O} - 12J_{Fe^OFe^T} + 2J_{YbFe^O}$
4	↑	↑	↑	↑	$E'_4 - E'_1 = -10J_{Fe^OFe^T} - 12J_{NiFe^T} + 8J_{Fe^TFe^T} - 2J_{YbFe^T}$

tetrahedral spin. Had the octahedral spins been antiparallel (represented by the dashed arrow), one of them would have been parallel to the tetrahedral spin. Since the strength of antiferromagnetic exchange interactions between the neighboring octahedral and tetrahedral spins are far stronger compared to that between neighboring spins (see Fig. 8), the octahedral spins are forced to align parallel to achieve the ground-state magnetic ordering as shown by the solid arrows.

To explain the effect of Yb spin-half-impurity on the host magnetic ordering, the exchange interaction strengths J_{YbFe^T}, J_{YbFe^O}, and J_{YbNi} along the paths shown in Fig. 7(b) were estimated. The equations listed in the bottom part of Table IV were used to estimate these magnetic interactions. Here, the effect of Yb^{3+} on the host-host spin interactions was neglected. The estimated Yb-host J_{ij}'s are listed in Table V.

From Table V, it is seen that Yb-Fe^T coupling is significantly weak (−3.73 meV) in comparison to that of the host octahedral-tetrahedral spin interactions: Fe^O-Fe^T (−36.52 meV) and Ni-Fe^T (−24.8 meV). At the same time, the Yb-Fe^O (−23.72 meV) and Yb-Ni (−23.05 meV) antiferromagnetic coupling have become stronger in comparison to that of the host octahedral-octahedral spin interactions: Fe^O-Fe^O (−19.12 meV) and Fe^O-Ni (−4.07 meV). Based on the coordination numbers of this inverse spinel structure, it was noted that there are four neighboring Yb-Ni (Fe^O-Ni), two neighboring Yb-Fe^O (Fe^O-Fe^O), and six neighboring Yb-Fe^T (Fe^O-Fe^T) magnetic interactions. From the subtraction $(2J_{YbFe^O} + 4J_{YbNi} + 6J_{YbFe^T}) - (2J_{Fe^OFe^O} + 4J_{Fe^ONi} + 6J_{Fe^OFe^T})$, it is found that there is a net decrease in the strength of the antiferromagnetic interaction by 7 meV/f.u. in the $NiFe_{2-0.0625}Yb_{0.0625}O_4$ compound, which in turn decreases the T_C.

IV. SUMMARY AND CONCLUSIONS

In summary, a combined experimental and theoretical study was carried out through XPS, ND, and magnetization measurements as well as spin-polarized DFT calculations to explain the electronic and magnetic structure of pure and Yb-substituted strongly correlated oxide, $NiFe_{2-x}Yb_xO_4$. The emphasis was on examining the strong correlation effect on the magnetic ordering of NFO and how the spin-half Yb impurity couples with the host to affect the magnetization and T_C of this inverse spinel ferrite.

The 3+ charge state of Yb (which substitutes the octahedral Fe) was confirmed from XPS measurements. The ND studies

TABLE V. The strength of exchange interactions J_{ij} for pure and Yb-substituted NFO. The values are obtained from the simultaneous solution of the equations of Table IV. For the purpose of comparison, the values from the literature are also listed here. Reference [37] has calculated J_{ij} per unpaired spin at each site. Hence the comparison is made with $S_iS_jJ_{ij}$, where S_i is the total number of unpaired spins at the ith site.

		J values in meV					
Type of interaction	Interaction distance (Å)	Present work	Three-sublattice model (Ref. [37])	Anderson transfer integral (Ref. [37])	Pseudopotential DFT (Ref. [38])	Yb substitution	Present work
J_{NiNi}	2.99	−13.77	10.32	9.99			
J_{NiFe^O}	2.99	−4.07	−2.32	−8.62	−3.80	J_{YbNi}	−23.05
J_{NiFe^T}	3.50	−24.80	−23.61	−23.61	−23.60		
$J_{Fe^TFe^T}$	3.60	−8.22	−32.25	−32.32			
$J_{Fe^OFe^O}$	2.99	−19.12	−11.62	−19.37		J_{YbFe^O}	−23.72
$J_{Fe^TFe^O}$	3.50	−36.52	−66.00	−60.32	−38.30	J_{YbFe^T}	−3.73

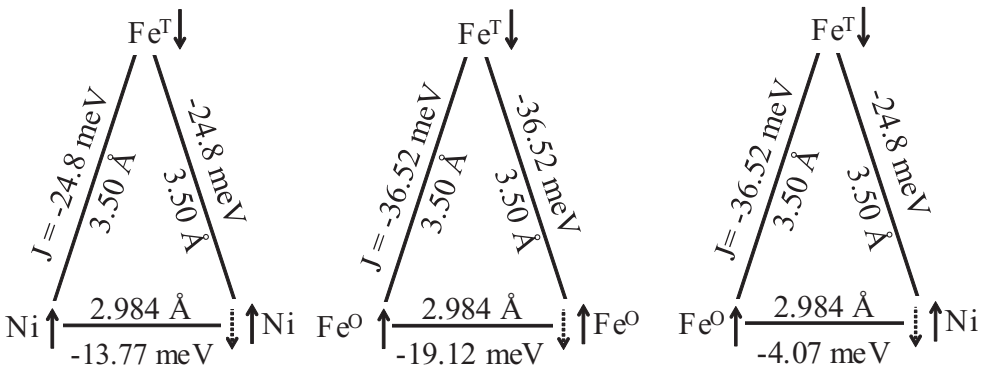

FIG. 8. Schematic of two neighboring octahedral spins joining the tetrahedral spin to form a triangle. The solid arrows indicate the ground-state magnetic ordering of that particular spin, whereas the dotted one is suggested by the J's as calculated from the above equations.

confirmed the ferrimagnetic ordering in NFO where spins at the octahedral sites (Ni^{2+} and Fe^{3+} cations) are aligned parallel while the spins at the tetrahedral sites (Fe^{3+} cations) are antiparallel to those at the octahedral sites. The magnetization measurements indicated a small decrease in the Curie temperature from 853 to 836 K with 7.5% Yb substitution. From the estimation of exchange interaction strengths, it was found that the spins at the octahedral sites preferred to align antiparallel. However, stronger antiferromagnetic coupling with the spins at the tetrahedral sites forces them to parallel in order to avoid spin frustration. By examining the effect of Hubbard U, it is concluded that this compound behaves as a mixed insulator under the Zaanen-Sawatzky-Allen classification scheme. Due to crystal-field effect and strong correlation effect, the Yb-$f_{z(x^2-y^2)}$ orbital carries the unpaired spin which, unlike in the pure case, strengthens the antiferromagnetic coupling with the neighboring spins at the octahedral sites and significantly weakens the same with the spins at the tetrahedral site. Based on the estimation of magnetic coupling between the impurity and host spins, it was found that there was a net decrease in the antiferromagnetic interaction strength, and as a consequence the T_C of the compound is decreased.

ACKNOWLEDGMENTS

The authors thank the HPCE facility at IIT Madras for computations and University Grants Commission Department of Atomic Energy Consortium for Scientific Research, Mumbai center, Bhabha Atomic Research Centre, Trombay, Mumbai-400 085 India for ND measurements. K.U. thanks Dr. Kamala Bharathi for the XPS measurements. The theoretical component of this work was supported by Department of Science and Technology through Grant No. EMR/2016/003791.

K.U. and S.S. contributed equally to this work.

[1] Z. Q. Wang, X. Y. Zhong, R. Yu, Z. Y. Cheng, and J. Zhu, Nat. Commun. **4**, 1395 (2013).
[2] S. Matzen, J.-B. Moussy, P. Wei, C. Gatel, J. C. Cezar, M. A. Arrio, P. Sainctavit, and J. S. Moodera, Appl. Phys. Lett. **104**, 182404 (2014).
[3] N. M. Caffrey, D. Fritsch, T. Archer, S. Sanvito, and C. Ederer, Phys. Rev. B **87**, 024419 (2013).
[4] U. Lüders, A. Barthélémy, M. Bibes, K. Bouzehouane, S. Fusil, E. Jacquet, J.-P. Contour, J.-F. Bobo, J. Fontcuberta, and A. Fert, Adv. Mater. **18**, 1733 (2006).
[5] V. K. Verma, V. R. Singh, K. Ishigami, G. Shibata, T. Harano, T. Kadono, A. Fujimori, F.-H. Chang, H.-J. Lin, D.-J. Huang, C. T. Chen, Y. Zhang, J. Liu, Y. Lin, C.-W. Nan, and A. Tanaka, Phys. Rev. B **89**, 115128 (2014).
[6] J. Chappert and R. B. Frankel, Phys. Rev. Lett. **19**, 570 (1967).
[7] K. Kamala Bharathi, K. Balamurugan, P. N. Santhosh, M. Pattabiraman, and G. Markandeyulu, Phys. Rev. B **77**, 172401 (2008).
[8] K. K. Bharathi, G. Markandeyulu, and C. V. Ramana, J. Phys. Chem. C **115**, 554 (2011).
[9] N. Rezlescu, E. Rezlescu, C. Pasnicu, and M. L. Craus, J. Phys.: Condens. Matter **6**, 5707 (1994).
[10] N. Rezlescu and E. Rezlescu, Solid State Commun. **88**, 139 (1993).
[11] E. Rezlescu, N. Rezlescu, P. D. Popa, L. Rezlescu, and C. Pasnicu, Phys. Status Solidi A **162**, 673 (1997).
[12] S. Chikazumi, *Physics of Ferromagnetism* (Oxford University Press, New York, 1997).
[13] J. Smit and H. P. J. Wijn, *Ferrites* (Philips Technical Library, Eindhoven, The Netherlands, 1959).
[14] K. Ugendar, V. R. Reddy, and G. Markandeyulu, IEEE Trans. Magn. **52**, 1 (2016).
[15] V. G. Ivanov, M. V. Abrashev, M. N. Iliev, M. M. Gospodinov, J. Meen, and M. I. Aroyo, Phys. Rev. B **82**, 024104 (2010).
[16] M. N. Iliev, D. Mazumdar, J. X. Ma, A. Gupta, F. Rigato, and J. Fontcuberta, Phys. Rev. B **83**, 014108 (2011).
[17] D. Fritsch and C. Ederer, Appl. Phys. Lett. **99**, 081916 (2011).
[18] J.-S. Chung, E.-J. Cho, and S.-J. Oh, Phys. Rev. B **41**, 5524 (1990).
[19] A. Yasui, S.-I. Fujimori, I. Kawasaki, T. Okane, Y. Takeda, Y. Saitoh, H. Yamagami, A. Sekiyama, R. Settai, T. D. Matsuda, Y. Haga, and Y. Onuki, J. Phys.: Conf. Ser. **273**, 012067 (2011).
[20] T. Droubay and S. A. Chambers, Phys. Rev. B **64**, 205414 (2001).

[21] S. Hüfner, *Photoelectron Spectroscopy—Princples and Applications* (Springer-Verlag, Berlin/Heidelberg, 1995).
[22] A. Fujimori and F. Minami, Phys. Rev. B **30**, 957 (1984).
[23] A. P. Grosvenor, M. C. Biesinger, R. S. Smart, and N. S. McIntyre, Surf. Sci. **600**, 1771 (2006).
[24] A. J. Signorelli and R. G. Hayes, Phys. Rev. B **8**, 81 (1973).
[25] S. B. M. Hagström, P. O. Hedén, and H. Löfgren, Solid State Commun. **8**, 1245 (1970).
[26] K. K. Bharathi and G. Markandeyulu, J. Appl. Phys. **103**, 07E309 (2008).
[27] P. Blaha, G. M. K. Schwarz, D. Kvasnicka, and J. Luitz, *WIEN2k: An Augmented Plane Wave Plus Local Orbitals Program for Calculating Crystal Properties* (TU Wien, Austria, 2001).
[28] D. Fritsch and C. Ederer, Phys. Rev. B **86**, 014406 (2012).
[29] M. Pénicaud, B. Siberchicot, C. Sommers, and J. Kübler, J. Magn. Magn. Mater. **103**, 212 (1992).
[30] Z. Szotek, W. M. Temmerman, D. Ködderitzsch, A. Svane, L. Petit, and H. Winter, Phys. Rev. B **74**, 174431 (2006).
[31] H. Perron, T. Mellier, C. Domain, J. Roques, E. Simoni, R. Drot, and H. Catalette, J. Phys.: Condens. Matter. **19**, 346219 (2007).
[32] Q.-C. Sun, H. Sims, D. Mazumdar, J. X. Ma, B. S. Holinsworth, K. R. O'Neal, G. Kim, W. H. Butler, A. Gupta, and J. L. Musfeldt, Phys. Rev. B **86**, 205106 (2012).
[33] S. L. Dudarev, G. A. Botton, S. Y. Savrasov, C. J. Humphreys, and A. P. Sutton, Phys. Rev. B **57**, 1505 (1998).
[34] V. N. Antonov, B. N. Harmon, and A. N. Yaresko, Phys. Rev. B **67**, 024417 (2003).
[35] D. Fritsch and C. Ederer, Phys. Rev. B **82**, 104117 (2010).
[36] J. Zaanen, G. A. Sawatzky, and J. W. Allen, Phys. Rev. Lett. **55**, 418 (1985).
[37] C. M. Srivastava, G. Srinivasan, and N. G. Nanadikar, Phys. Rev. B **19**, 499 (1979).
[38] C. Cheng, J. Magn. Magn. Mater. **325**, 144 (2013).
[39] P. W. Anderson, *Magnetism* (Academic, New York, 1963), Vol. I.